Eur. Phys. J. E **19**, 453–459 (2006)
DOI 10.1140/epje/i2005-10069-7

THE EUROPEAN PHYSICAL JOURNAL E

Measurement of adhesion energies and Young's modulus in thin polymer films using a novel axi-symmetric peel test geometry

A.N. Raegen[1], K. Dalnoki-Veress[1,a], K.-T. Wan[2], and R.A.L. Jones[3]

[1] Department of Physics & Astronomy, McMaster University, Hamilton, ON, Canada
[2] Department of Mechanical and Aerospace Engineering, University of Missouri-Rolla, Rolla, MO 65409, USA
[3] Department of Physics & Astronomy, University of Sheffield, Sheffield, UK

Received 14 October 2005 /
Published online: 18 April 2006 – © EDP Sciences / Società Italiana di Fisica / Springer-Verlag 2006

Abstract. We present a novel method of probing adhesion energies of solids, particularly polymers. This method uses the axi-symmetric deformation of a thin spincast polymer membrane brought into contact with a flat substrate to probe the work of adhesion. The use of a thin membrane minimizes uncertainty in the radius of contact, while the use of spincast films provides very smooth surfaces by means of a very simple method. The experimental profile of the deformed membrane shows good agreement with the expected logarithmic profile. The experimental setup enables the measurement of Young's modulus and the solid-solid work of adhesion for thin films. The value obtained for Young's modulus of polystyrene (PS) was found to be in agreement with other conventional measurement techniques. In addition, measurement of the work of adhesion at the PS/silicon oxide interface was possible. The apparatus is well suited to studying the dependence of Young's modulus, work of adhesion and fracture energy on membrane thickness, temperature, pulling rate, and ageing of the interface, and can readily be modified to study biologically relevant samples.

PACS. 68.35.-p Solid surfaces and solid-solid interfaces: Structure and energetics – 68.60.Bs Mechanical and acoustical properties – 82.35.Gh Polymers on surfaces; adhesion – 82.35.Lr Physical properties of polymers

Introduction

Current methods of measuring surface forces can be divided into two basic categories: experiments closely related to the peel test [1–5] or to JKR measurements [1,2,6–15], which are based upon the original theory by Johnson, Kendall, and Roberts [6]. In peel test experiments, a strip of known width is peeled from a surface while the force required to propagate the contact line (crack) is observed. The measurements can provide a measure of the *fracture energy* of the interface (energy cost in creating new surfaces). The JKR-type experiments can be used to measure the *adhesion energy* (energy gain in bringing surfaces into contact) as well as the fracture energy of samples. JKR experiments are often performed by bringing a solid, elastic hemisphere into contact with a hard flat substrate. In the JKR setup, a free energy balance is obtained between the energy gain in having two surfaces come into contact, the energy cost of deforming the samples, and the mechanical potential energy of the applied load. An extension of the JKR-type experiments is the surface forces apparatus (SFA). The SFA employs two crossed cylinders and provides force measurement capabilities sensitive enough to measure surface forces without actual contact between the substrates. Very fine measurements of adhesion, friction, and fracture between surfaces are possible with the SFA [2,9–12].

JKR experiments, while able to measure both the adhesion and fracture energies, do have some drawbacks. Since JKR involves the deformation of geometrically incompatible solid bodies, often with fairly large elastic moduli, large forces are frequently needed to obtain appreciable contact. Even with the use of elastic hemispheres, the contact area may be small, which contributes to uncertainty in the values of adhesion energy. In order to have appreciable contact, the polymer of interest is often a thin coating on an elastic hemisphere, with the assumption that the hemisphere dominates the physical properties of deformation. The thickness of the polymer layer is not rigorously included in the JKR theory, although it is included in other adhesion geometries [5]. In addition, bulk casting methods are often used to form the hemispheres, so surface roughness may be problematic, depending upon the method and polymer used. This can

[a] e-mail: dalnoki@mcmaster.ca

be alleviated in PDMS by depositing small droplets of the polymer on glass slides prior to crosslinking. The liquid droplets take the shape of a spherical cap, which they retain after crosslinking [13]. By replacing the hemisphere with a spincast free-standing film, the entire membrane deforms. Because a thin membrane is more compliant than a solid hemisphere a larger contact patch is obtained than when a hemisphere is used. The benefit of this is twofold: 1) The contact area, which is squared when calculating surface energies, has a small relative uncertainty because of its large size. 2) Smaller surface energies can be measured because the measured force scales like the area of the contact patch. Perhaps most important is that the use of spincast films can greatly decrease the surface roughness of the substrates, as well as provide an alternate method of preparing suitable samples.

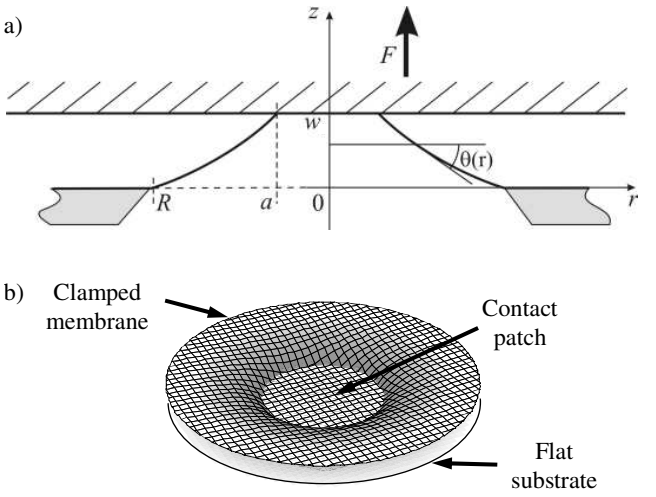

Fig. 1. a) Schematic of a membrane with a circular patch in contact with a flat substrate. b) The topography of a membrane in contact with a flat substrate.

Theory

The theory for a membrane in contact with a substrate has been discussed by several authors [4,15–21]. Wan and co-workers developed the theory for a range of different geometries, including rectangular [17,19] and circular [18, 19] punches in contact with a membrane. Preliminary experimental results for these geometries were presented for the case of commercially available tape [17,19]. Wan also modelled circular [20,21] and rectangular [20] *pre-stressed* membranes brought into contact with flat substrates. In the following we recap some of the results obtained for the theory for the pre-stressed, circular membrane brought into contact with a flat substrate (see Fig. 1) [20,21]. The equations required for the analysis of the experimental results are presented here and are slightly different from what has appeared previously [22]. The calculation follows work done by others; however, since the detailed calculation does not appear in the literature for this applicable case the complete derivation appears in the appendix.

A washer supports a circular membrane (free-standing polymer film) with radius R. A flat substrate in contact with the membrane is pulled to a distance w by a force F and the radius of the contact patch is a. As the punch is pulled away from the membrane, the total tension in the film is given by $T = T_0 + T_m$, where T_0 is the pretension present as a result of sample preparation and T_m the *concomitant* tension (the change in tension of the membrane that arises from increasing w). T is equal to the radial stress, σ_r, multiplied by the thickness of the membrane, h.

We assume that the deformation of the membrane is entirely dominated by elastic stretching, rather than bending. This is a valid assumption since the bending energy is negligible compared to the stretching energy in a very thin ($h \sim 0.4\,\mu$m) film of large radius ($R = 1.5\,$mm). For this case it can be shown that the film profile, $z(r)$, is the same minimal surface as a soap bubble between two axi-symmetric rings [4,15,16,18–21]:

$$z(r) = w\frac{\ln(R/r)}{\ln(R/a)}. \qquad (1)$$

Using this profile, and for small deformations, the force is given by

$$F = \frac{\pi E' h}{(R^2 - a^2)\big[\ln(R/a)\big]^2} w^3 + \frac{2\pi T_0}{\ln(R/a)} w, \qquad (2)$$

where $E' = E/(1-\nu)$, E is Young's modulus, and ν is Poisson's ratio of the membrane (*note that the form of E' is different from what is often used for thick plates*, see [23]). The first term is due to the change in stress as the free-standing film is pulled away from the substrate, and the second is due solely to the pre-stress. The work of adhesion (W) can be shown to be

$$W = -\frac{E' h}{4}\frac{R^2 - a^2 + a^2\ln(R/a)}{a^2\big[\ln(R/a)\big]^3(R^2-a^2)^2} w_0^4 - \frac{T_0}{2a^2\big[\ln(R/a)\big]^2} w_0^2, \qquad (3)$$

where $W = \gamma_1 + \gamma_2 - \gamma_{12}$ (*i.e.* the Dupré energy), γ_1 and γ_2 are the surface energies of the two surfaces and γ_{12} is the interfacial energy of the pair, and w_0 is the original separation at which equilibration occurred. In the experiment, R, a, w, and h are easily obtained. By measuring F as a function of w, and performing a two-parameter fit to equation (2), E' and T_0 can be determined, thereby providing all the necessary information to calculate W from equation (3).

Experimental

Films of high molecular weight (1410 kg/mol), low polydispersity ($M_n/M_w = 1.05$) polystyrene (PS) (Polymer Source, Dorval, Quebec, Canada) were spincast out of toluene solutions. The adhesion substrates used were cleaned silicon with native oxide layer (the cleaning procedure consisted of removing particulates with a CO_2 jet,

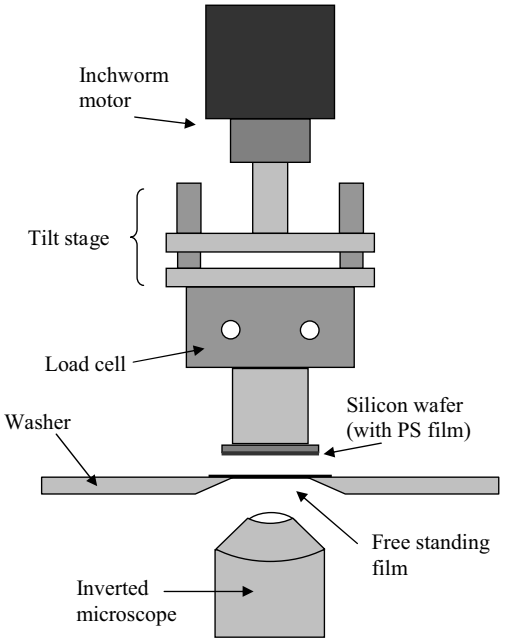

Fig. 2. Schematic of the experimental apparatus.

followed by a rinse with Milli-Q water, acetone, and filtered toluene). Free-standing films were made by spincasting PS onto freshly cleaved mica, with film thicknesses of $\sim$ 300 nm, $\sim$ 400 nm, and $\sim$ 440 nm. Samples were annealed in vacuum at 130 °C ($\sim$ 30 degrees above the glass transition for PS) for at least 24 hours to remove residual solvent and relax the chains. The films were cooled to room temperature at a slow rate $\sim$ 1 °C/min, floated onto a water surface, captured across a 3 mm diameter hole in a stainless steel holder, and then dried in air. The free-standing films are often not taut over the sample holder and may have small undulations due to the transfer process (we note that such samples will not produce a circular contact patch which is a requirement of the method presented). In order to ensure taut membranes with a uniform pre-stress, the samples were heated (Linkam hot stage) above T_g for a short period of time ($\sim$ 10 min at $\sim$ 110 °C), while observing the sample with an optical microscope until the undulations had disappeared (the polymer film, while in the melt, will become taut due to the surface tension of the liquid). Besides ensuring that an undulation-free membrane is obtained, this annealing step also encourages strong adhesion between the film and washer, thereby avoiding delamination of the membrane from the sample holder. Samples were then cooled at 10 °C/min to give the films the same thermal history. Due to differential expansion between the stainless steel sample holder and the film, once cooled, the membrane is under tension (*i.e.* the stainless steel has a smaller expansion coefficient than the polymer film). During all stages of sample preparation, great care was taken to ensure the interacting surfaces remained clean (use of Milli-Q water, filters, laminar flow hood, etc.).

In Figure 2 a schematic diagram of the experimental apparatus is shown. Flat substrates are mounted on a Transducer Techniques SGO Series 50 gram Load Cell, which is attached via a Newport MM-1 tilt stage to a Burleigh Inchworm linear stepper motor. This module is mounted axi-symmetrically above the free-standing film, atop an Olympus IX70 inverted microscope equipped with a Pixelink CCD camera. The entire apparatus is placed on a Halcyonics MOD-1 anti-vibration table. A bandpass filter at either 630, 530, or 460 nm was used to observe interference fringes set up between the two films, and to enhance the visibility of the contact patch as needed (more on the use of the filters below). A Labview program enables control of the motor and automation of image capture and data acquisition.

Results and discussion

Films were first brought together quickly by manually advancing the motor to a small (tenths of a millimetre) separation. At this small separation, the films are observed using monochromatic light (an expanded laser beam at 632 nm), which sets up interference fringes. The fringes enable the films to be levelled with respect to one another using the tilt stage (see Fig. 2). Once the films are levelled and brought to a separation of a few tens of microns (observed by manually changing the focus of the microscope), contact is initiated using an air jet to gently push the membrane towards the substrate (see Fig. 3). The resultant contact patch is circular and centred, giving an ideal axi-symmetric geometry. We note that the initial contact patch, as a result of the air jet, is small. It is the surface energy that drives the contact patch to grow to some equilibrium value.

Once equilibrium is reached (which is achieved rapidly), the radius of the contact patch was obtained by analyzing pictures taken at low magnification. Determination of the absolute separation was carried out in two ways. By focusing on the contact line with a high powered objective, then focusing on the film where it contacts the washer, the separation is given by the distance traveled in manually changing the focus of the microscope. An alternative method was also used, which proves the validity of equation (1) and the assumption that the film can be treated as an elastic membrane (*i.e.* elastic bending can be ignored). The region near the contact patch is illuminated under the microscope while using a bandpass filter. Bandpass filters, at 630, 530, or 460 nm, for red, green, and blue, are used with one chosen for exhibiting good contrast between the contact patch and free-standing annulus. In Figure 4, a representative image is shown which clearly shows the interference fringes. From the radial intensity (see Fig. 5), the film profile is obtained (see Fig. 6). The film profile can be fit to equation (1), allowing for determination of the separation. While this provides an excellent method of determining separation, more exciting is the fact that one can fit equation (1) to the profile obtained from the interference fringes. The profile of the film was found to be in excellent agreement with the expected logarithmic profile [4,15,16,18]. Both methods of finding the

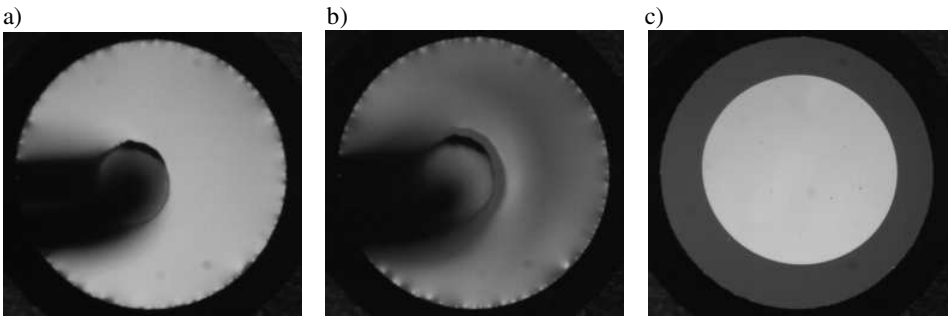

Fig. 3. A series of images showing how the films are brought into contact. Both substrate and membrane films are about 200 nm thick, and the hole (large ring) in the sample holder is 3 mm in diameter. The large dark object entering on the left of the images is a small tube used to provide an air jet. a) Films at small separation. b) An air jet is used to bow the membrane. c) Contact is made, and grows to some equilibrium radius.

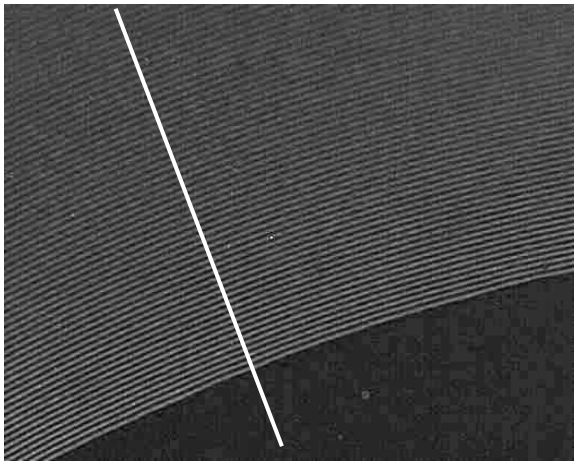

Fig. 4. Interference fringes set up between the two films are observed using a choice of bandpass filters (630 nm in this case). The vertical distance between each fringe is half the wavelength used to observe the films.

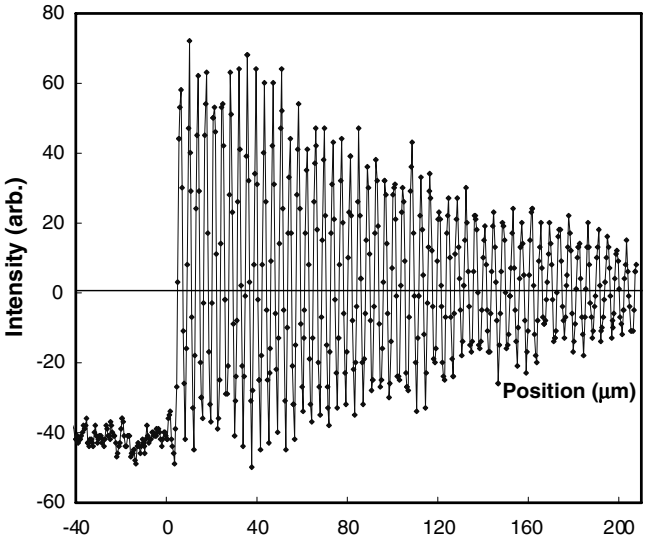

Fig. 5. Data from the interference fringes in Figure 4. The intensity values of pixels along a line perpendicular to the contact line are plotted *versus* distance away from the contact line. Zero crossings of this plot can be used to obtain the membrane profile.

separation (*i.e.* focussing on the films, membrane profile determination) are in agreement.

After equilibration and measurement of the contact parameters, the films are pulled apart at a fixed rate ($\sim 0.1\,\mu$m/s), while monitoring the force and separation (see Fig. 7). Through most of the pulling run, the contact patch does not decrease in size as a result of the increased force. The contact patch is fixed because the energy gained by bringing the surfaces together (work of adhesion) is less than the cost of pulling them apart (fracture energy). This hysteresis is typical of adhesion measurements [2,7–11,14,15].

During the first stage of the run ($w \lesssim 90\,\mu$m) the constitutive relation is entirely governed by elastic stretching. To check for plastic deformation in this stage, we have pulled the films apart and returned to the original separation while monitoring the force. This can be done repeatedly, increasing the pulling distance of each loop, up to a maximum travel distance ($w - w_0$) of $\sim$ 40 to $\sim 70\,\mu$m, depending upon the thickness of the film and contact parameters, before the onset of plastic losses. The point at which the free-standing annulus crosses into the plastic regime is exhibited in the following ways. 1) The relaxing constitutive relation will show deviation from the previous pulling relation. 2) In an extended pulling run, there is an obvious kink in the constitutive relation, as shown in Figure 7 at $w \sim 90\,\mu$m. 3) The onset of plastic behaviour can also be observed visually, manifested in crack-like structures (necks, crazes, or shear deformation zones) beginning at the contact line and propagating outward. In order to determine the pretension, Young's modulus, and the work of adhesion, only the data prior to the point at which plastic behaviour is observed is used, as indicated by the fit of the data to equation (2) shown in Figure 7 (*i.e.* only data in the elastic regime is used). The contact patch is found to remain unchanged until a separation that can be well beyond the distance required for plastic behaviour ($w \sim 177\,\mu$m in Fig. 7). Once the fracture energy is reached, the membrane detaches from the film either all at once or in stages, depending upon

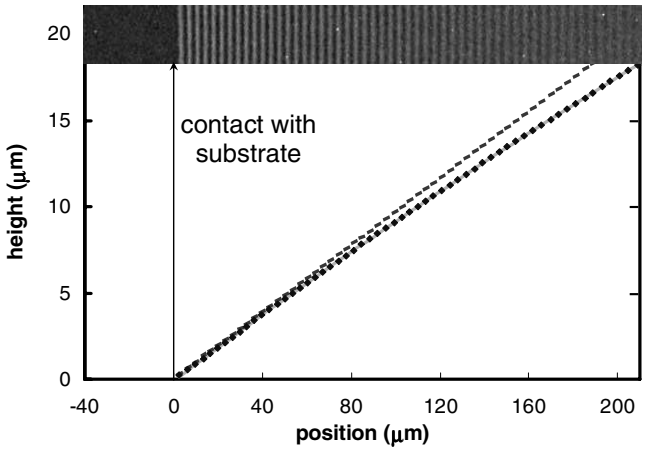

Fig. 6. The profile obtained by assigning heights to the zero crossings in Figure 5. This profile shows excellent agreement with the logarithmic profile expected in the theory. By fitting a curve (solid line), the derivative of the fit at the contact line gives the contact angle (dotted line).

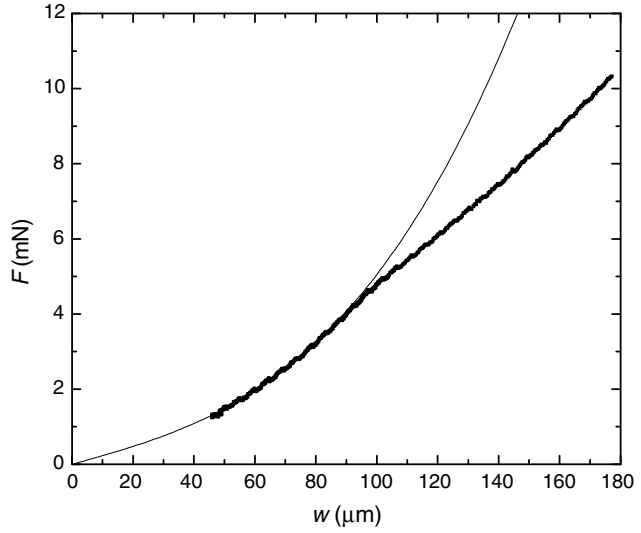

Fig. 7. A constitutive relation plot for a PS/SiO_x system, showing a full pulling run and the fit to the expected non-Hookian relation. Young's modulus was found to be 4.7 ± 0.3 GPa.

the stability of a smaller contact patch and the possibility of further plastic deformations as the contact shrinks.

We re-iterate that there are two stages to the experiment. In the first stage contact is initiated at some value of w_0 (typically ~ 50 microns), the contact patch reaches an equilibrium radius a (from 0.5 mm to 1 mm) and an equilibrium force (~ 0.002 N). These quantities are not sufficient to determine the Dupré work of adhesion, W, as is clear from equation (3). In the second stage the separation is increased thereby obtaining F as a function of w. A fit using equation (2) is performed to the elastic regime allowing Young's modulus, the pretension, and thus W to be obtained. Typical values of the pretension and concomitant tension at equilibration are 5 N/m and 1.5 N/m, respectively. The Dupré work of adhesion is obtained from the equilibrium values of F, w_0 and a after the contact patch has spread (*i.e.* the first data point in Fig. 7). The point at which the kink occurs in the constitutive relation is when the constitutive relation reaches ~ 5 N/m. Though we do not present the results here, it is also possible to obtain the fracture energy, W_f. W_f can be obtained from where the contact patch first starts to delaminate upon increasing w_0 (*i.e.* the contact patch becomes unstable). The crucial assumption to measuring W_f is that there is no plastic deformation of the membrane. Such measurements will appear in a future publication.

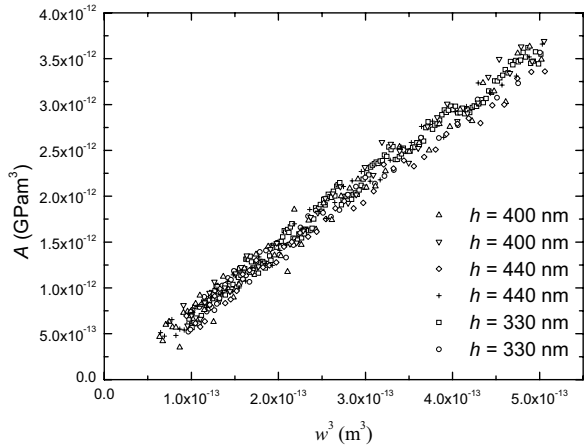

Fig. 8. A plot of 6 PS/SiO_x experimental runs normalized according to equation (4), showing the reproducibility of the technique. The slope of the data is $E' = E/(1-\nu) = 7.1 \pm 0.4$ GPa.

We measure E' to be 7.1 ± 0.4 GPa. Literature values of Poisson's ratio of polystyrene are quoted to be ~ 0.33 [24]. Assuming that bulk values of Poisson's ratio are valid for thin films ($\sim$ 300–440 nm), we measure E to be 4.7 ± 0.3 GPa. While fitting the data in the elastic regime to the theoretical constitutive relation (Eq. (2)) we find that both terms in equation (2) are required for a satisfactory fit. Equation (2) can be rearranged such that the slope of the data corresponds to E':

$$A \equiv \left[F - \frac{2\pi T_0}{\ln(R/a)} w\right] \frac{(R^2 - a^2)\left[\ln(R/a)\right]^2}{\pi h} = E' w^3. \quad (4)$$

In Figure 8 is shown a plot of A as a function of w^3 for six samples of the PS/SiO_x system. Clearly, the consistency between the different samples indicates that there is no dependence on film thickness over this range, within experimental uncertainty. Since the pretension T_0 and E' are obtained from the fit of the data to equation (2), and all other parameters are also known from the experiment, equation (3) can be used to obtain the work of adhesion W. Experimentally, we find the work of adhesion of the PS/SiO_x interface to be 21 ± 3 mN/m. The bulk of the uncertainty in the experimental values come not from error in measurement of the contact radius, washer radius, but from uncertainty in the separation w. Current studies are underway to reduce this error in order to provide higher-resolution measurements.

Excellent agreement was found in all our measurements with equation (2) (see the solid line in Fig. 7). The fit of the data to equation (2) enables the determination of the pretension, T_0, which is required for the measurement of the work of adhesion, as well as E'. Since $E' = E/(1-\nu)$ and assuming Poisson's ratio from the literature, this procedure provides a very simple method to measure Young's modulus of thin free-standing films. Given the current interest in thin polymer films, polymer confinement, and finite-size effects, such measurements are currently underway.

Conclusions

We have measured solid-solid adhesion energies for polystyrene membranes brought into contact with flat, rigid substrates. The experimental method discussed produced several results: 1) Excellent agreement with the expected membrane profile was observed. This proves the validity of the theory as well as the assumption that the thin films can be treated as elastic membranes without the inclusion of a bending energy term. 2) Young's modulus, E can be readily obtained assuming a known value of Poisson's ratio and is in agreement with [24]. 3) The work of adhesion is easily measured with this technique. The novel axi-symmetric geometry presented offers some advantages over other conventional techniques, with the potential for higher accuracy measurements on reliably smooth surfaces. This apparatus is well suited to exploring solid-solid adhesion dependence on film thickness, temperature, molecular weight, ageing, environment, pulling dynamics, and the technique can be readily extended to employ biologically relevant samples (*i.e.* biological tissues, dermo-prosthesis, retina detachment, lipid bilayers, etc.).

The authors acknowledge fruitful discussions with Professors Ken Shull and James Forrest. Financial support from NSERC, PREA, CFI, and OIT of Canada is gratefully acknowledged. Support for KTW from NSF CMS-0527912 is acknowledged.

Appendix A.

Here we provide a detailed derivation and clarify the basic assumptions that lead to the equations required for the analysis of the membrane– and flat-substrate–type experiment.

The geometry of the film and substrate system and relevant symbols are shown in Figure 1. A flat substrate is pulled to a distance w by a force F and the radius of the contact patch is a. In a thin membrane the bending energy is a negligible contribution compared to stretching, and the total tension in the membrane, T (a force per unit length), is made up of the sum of two contributions: T_0, the pretension present as a result of sample preparation and T_m, the concomitant tension. In equilibrium, all forces normal to the flat substrate are balanced, requiring:

$$F = 2\pi T r \sin\theta(r) = 2\pi T r \frac{-\partial z(r)}{\partial r}\,, \qquad \text{(A.1)}$$

where F is measured along the symmetric axis (*i.e.* perpendicular to the flat substrate), $\theta(r)$ and $z(r)$ are the angle relative to the flat substrate and the height of the film at position r, and we have made use of the small-angle approximation since the deformations are small. Integrating equation (A.1) and making use of the boundary conditions at a and R, the profile is found to be the same minimal surface as a soap film between two axi-symmetric rings [4, 15,16,18–21]:

$$z(r) = \frac{F}{2\pi T}\ln(R/r) = w\frac{\ln(R/r)}{\ln(R/a)}\,. \qquad \text{(A.2)}$$

Hooke's Law states that

$$E\varepsilon_r = \sigma_r - \nu\sigma_t \quad \text{and} \quad E\varepsilon_t = \sigma_t - \nu\sigma_r, \qquad \text{(A.3)}$$

where E is Young's modulus, ε is the strain on the film, ν is Poisson's ratio, σ is the stress, and the subscripts t and r refer to the tangential and radial components. From equation (A.3) we can obtain the concomitant tension (*i.e.* the tension in the membrane as a result of changing the distance w),

$$T_m = \sigma_r h = \frac{Eh}{1-\nu^2}(\varepsilon_r + \nu\varepsilon_t), \qquad \text{(A.4)}$$

In order to evaluate the term $(\varepsilon_r + \nu\varepsilon_t)$ we take the approach of Williams [4] and make two important assumptions. First of all, the membrane is taken to be ideal and hence does not support shear. If the membrane does not support a shear then the stress in the two orthogonal directions must be equal, $\sigma_r = \sigma_t$, or equivalently $\varepsilon_r = \varepsilon_t$. The second assumption is that the strains, which vary across the membrane, can be replaced by a constant average value:

$$\int_a^R 2\bar{\varepsilon}\,2\pi r\mathrm{d}r = \int_a^R \big(\varepsilon_r(r) + \varepsilon_t(r)\big)2\pi r\mathrm{d}r. \qquad \text{(A.5)}$$

These are very reasonable assumptions for the measurements presented since the film's thickness ($h \sim 0.4\,\mu$m) and the total displacement ($w \sim 100\,\mu$m) are both very small compared to the radius of the membrane ($R = 1.5$ mm). Considering a small radial and tangential linear element on the membrane before and after deformation, it is straightforward to show that (see Sect. 96 in [25]),

$$\varepsilon_r = \frac{\mathrm{d}u}{\mathrm{d}r} + \frac{1}{2}\left(\frac{\mathrm{d}w}{\mathrm{d}r}\right)^2 \quad \text{and} \quad \varepsilon_t = \frac{u}{r}\,, \qquad \text{(A.6)}$$

where w and u denote the displacement of the membrane in the z and r directions. Upon substitution of

equations (A.6) and (A.2) into (A.5) we obtain

$$\int_a^R 2\bar{\varepsilon} r \mathrm{d}r = \frac{1}{2}\int_a^R \left(\frac{\mathrm{d}z}{\mathrm{d}r}\right)^2 r\mathrm{d}r \Rightarrow$$
$$\bar{\varepsilon} = \frac{1}{2}\frac{w^2}{\ln(R/a)(R^2-a^2)} \sim \varepsilon_r = \varepsilon_t. \quad \text{(A.7)}$$

From equations (A.1) and (A.2) the force can then be written as

$$\begin{aligned} F &= \frac{2\pi w}{\ln(R/a)}(T_0 + T_m) \\ &= \frac{2\pi w}{\ln(R/a)}\left(T_0 + \frac{E'hw^2}{2(R^2-a^2)\ln(R/a)}\right) \\ &= \frac{\pi E'h}{(R^2-a^2)[\ln(R/a)]^2}w^3 + \frac{2\pi T_0}{\ln(R/a)}w \\ &= \alpha w^3 + \beta w, \end{aligned} \quad \text{(A.8)}$$

where $E' = E/(1-\nu)$ and for simplicity we have defined the pre-factors $\alpha(a)$ and $\beta(a)$. The first term is due to the change in stress as the free-standing film is pulled away from the substrate, and the second is due solely to the pre-stress. We follow the same formalism as in the JKR theory [6,20,21], with the total energy (U_t) being equal to the mechanical potential energy of the applied load ($U_m = Fw$) put into the system, minus the energy output which consists of the elastic energy of deformation ($U_e = \int F\mathrm{d}w$), and the surface energy term ($U_s = \pi a^2 W$). At equilibrium we have the condition that

$$\mathrm{d}U_t = 0 = F\mathrm{d}w - \mathrm{d}U_s - \mathrm{d}U_e,$$

and since we are looking for the equilibrium radius of the contact patch,

$$\begin{aligned} \frac{\mathrm{d}(U_t)}{\mathrm{d}a} = 0 &= F\frac{\mathrm{d}w}{\mathrm{d}a} - \frac{\mathrm{d}U_s}{\mathrm{d}a} - \frac{\mathrm{d}U_e}{\mathrm{d}a} \\ &= F\frac{\mathrm{d}w}{\mathrm{d}a} - 2\pi a W - \frac{\mathrm{d}}{\mathrm{d}a}\left(\alpha\frac{w^4}{4} + \beta\frac{w^2}{2}\right). \end{aligned} \quad \text{(A.9)}$$

In the present study, the experiment is carried out in the *fixed-grips* configuration (w_0 is constant), where the displacement, w_0, is controlled and F is measured. Since the displacement is held fixed, while F and a change to reach equilibrium, $\mathrm{d}w_0/\mathrm{d}a = 0$ and equation (A.9) becomes

$$0 = -2\pi a W - \frac{w_0^4}{4}\frac{\mathrm{d}\alpha}{\mathrm{d}a} - \frac{w_0^2}{2}\frac{\mathrm{d}\beta}{\mathrm{d}a},$$

or

$$W = -\frac{w_0^4}{8\pi a}\frac{\mathrm{d}\alpha}{\mathrm{d}a} - \frac{w_0^2}{4\pi a}\frac{\mathrm{d}\beta}{\mathrm{d}a}. \quad \text{(A.10)}$$

It is also possible to carry out an experiment in a *fixed-load* configuration, where the applied force is held constant and thus w and a change to reach equilibrium. In this case, $\mathrm{d}F/\mathrm{d}a = 0$ and equation (A.9) can be written as

$$\begin{aligned} 0 &= F\frac{\mathrm{d}w}{\mathrm{d}a} - 2\pi a W - \frac{\alpha}{4}\frac{\mathrm{d}w^4}{\mathrm{d}a} - \frac{w^4}{4}\frac{\mathrm{d}\alpha}{\mathrm{d}a} - \frac{\beta}{2}\frac{\mathrm{d}w^2}{\mathrm{d}a} - \frac{w^2}{2}\frac{\mathrm{d}\beta}{\mathrm{d}a} \\ &= -2\pi a W - \frac{w^4}{4}\frac{\mathrm{d}\alpha}{\mathrm{d}a} - \frac{w^2}{2}\frac{\mathrm{d}\beta}{\mathrm{d}a}, \end{aligned}$$

which is equivalent to (A.10) when evaluated at w_0. This is to be expected since the approach to equilibrium (*i.e.* fixed w_0 or fixed F) should not determine the outcome. Evaluation of $\mathrm{d}\alpha/\mathrm{d}a$ and $\mathrm{d}\beta/\mathrm{d}a$, and substitution into equation (A.10) gives the final expression

$$\begin{aligned} W = &-\frac{E'h}{4}\frac{R^2 - a^2 + a^2\ln(R/a)}{a^2\left[\ln(R/a)\right]^3(R^2-a^2)^2}w_0^4 \\ &-\frac{T_0}{2a^2\left[\ln(R/a)\right]^2}w_0^2. \end{aligned} \quad \text{(A.11)}$$

References

1. K. Kendall, J. Phys. D **4**, 1186 (1971).
2. K. Kendall, *Molecular Adhesion and Its Applications* (Kluwer Academic/Plenum Publishers, New York, 2001).
3. J.G. Williams, J. Adhesion **41**, 225 (1993).
4. J.G. Williams, Int. J. Fract. **87**, 265 (1997).
5. A. Ghatak, L. Mahadevan, M.K. Chaudhury, Langmuir **21**, 1277 (2005).
6. K.L. Johnson, K. Kendall, A.D. Roberts, Proc. R. Soc. London, Ser. A **324**, 301 (1971).
7. V. Mangipudi, E. Huang, M. Tirrell, Macromol. Symp. **102**, 131 (1996).
8. M. Tirrell, Langmuir **12**, 4548 (1996).
9. M. Israelachvili, *Intermolecular & Surface Forces* (Academic Press Limited, London, 1992).
10. G. Luengo, J. Pan, M. Heuberger, J.N. Israelachvili, Langmuir **14**, 3873 (1998).
11. N. Maeda, N. Chen, M. Tirrell, J.N. Israelachvili, Science **297**, 379 (2002).
12. X. Zhang, Y. Zhu, S. Granick, Science **295**, 663 (2002).
13. K. Vorvolakos, M.K. Chaudhury, Langmuir **17**, 6778 (2003).
14. K.R. Shull, D. Ahn, W.-L. Chen, C.M. Flanigan, A.J. Crosby, Macromol. Chem. Phys. **199**, 489 (1998).
15. K.R. Shull, Mater. Sci. Eng. R **36**, 1 (2002).
16. M.E.R. Shanahan, C. R. Acad. Sci. Paris Ser. IV **1**, 517 (2000).
17. K.-T. Wan, J. Duan, J. Appl. Mech. **69**, 104 (2002).
18. K.-T. Wan, J. Appl. Mech. **69**, 110 (2002).
19. J. Duan, K.-T. Wan, K.-S. Chian, Thin Solid Films **424**, 120 (2003).
20. K.-T. Wan, D.A. Dillard, J. Adhes. **79**, 123 (2003).
21. K.-T. Wan, L. Kogut, J. Micromech. Microeng. **15**, 778 (2005).
22. There is some confusion in the expressions derived for adhesion energy in the previous publications (cf. Ref. [18] and K.-T. Wan, J. Adhes. **75**, 369 (2001)). The correct version is derived in the appendix.
23. K.-T. Wan, S. Guo, D.A. Dillard, Thin Solid Films **425**, 150 (2003).
24. J. Brandrup, E.H. Immergut, E.A. Grulke, *Polymer Handbook*, 4th edition (Wiley, New York, 1999).
25. S.P. Timoshenko, S. Woinowsky-Krieger, *Theory of Plates and Shells*, 2nd edition (McGraw-Hill, New York, 1959).